Measurements of Breakdown Voltage Characteristics of Medium Voltage Vacuum Circuit Breaker after Current Interruption

Szymon Stoczko, *Member, IEEE*, Marcin Szewczyk, *Senior Member, IEEE*, Waldemar Chmielak, Radosław Szreder, Zbigniew Pochanke

***Abstract*— We present a test circuit for measuring the breakdown voltage characteristics of a vacuum circuit breaker after current interruption process. The test circuit combines the high current part from the synthetic test circuit as per IEC Std. 62271-101 with the so-called Rabus high voltage part. The high current part reproduces the current phase before voltage build-up occurring after zero current crossing, then the Rabus high voltage part provides voltage breakdowns constituting breakdown voltage characteristics. The high current part can be adjusted to represent the actual current conditions which influences the physical conditions of the contact system upon which the interruption process is highly dependent. To illustrate the measuring system and the measuring procedure, the measurements of the breakdown voltages are reported for a commercial 12kV/1250A/31.5kA vacuum circuit breaker. The breakdown voltages are measured primarily as a function of time and then converted via a contact travel curve into the vacuum interrupter contact gap function. This allows the results to be converted back and applied to a breaker with the same characteristics of the vacuum interrupter unit operating in similar current conditions, but with different mechanical characteristics of the breaker-specific actuator than the one used in testing.**

***Index Terms*—vacuum circuit breakers, vacuum interrupters, voltage breakdowns, breakdown voltage characteristics, current interruption process.**

I. Introduction

Vacuum Interrupters (VIs) are a mature technology for current switching that dominates the medium voltage product segment of distribution breakers, and they have also found their way into low power generator and low-end of high voltage circuit breakers [1]. This is due to the VIs high reliability, long designed operational lifetime (20-30 years and beyond) and high-pressure tightness [2]. From the interior design perspective, the VIs are constantly researched towards anode [3] and cathode [4] spots development processes, contact gap phenomena [5] and late breakdowns observations [6]. The late breakdowns occurring after switching arc interruption cause a strong and potentially harmful interaction between the VCB and other power system components due to the high-frequency transients produced by the repetitive voltage breakdowns inside the VI contact system.

The voltage breakdowns in the VIs are initiated by residual and pre-breakdown electrons that are either existing in the contact gap after the foregoing breakdown process or are being supplied to the contact gap from the contacts due to the quantum field emission processes from the micro projections on the cathode contact surface and melting processes of the switching arc. Due to the VI very low operational pressure of 10^{-4} Pa and a typical contact gap (of 10-15 mm for the VI rated at 12 kV), the mean free path of the molecules is in the order of the VI external dimension. Therefore, the electrons that are subjected to acceleration in the electric field between the contacts hit the anode surface with the energy that is high enough to release the adsorbed gases and metal vapor from the anode surface. These molecules are then subjected to ionization processes which consequently establish the arc plasma channel between the entire contact gap [7]. These effects are related to the inherent design of the VI and the switching process, and therefore cannot be avoided in VCB technology.

From the system perspective the repetitive voltage breakdowns occurring during switching operation of VCB create high frequency transient overvoltages with frequency components up to several MHz and large values of voltage steepness up to 200 kV/us at full operational voltage [8]. They can threaten insulation systems of distribution transformers [8], wind turbine transformers [9], arc furnace transformers [10]; which is due to an uneven distribution of steep voltages along the windings [11]. The high frequency transients due to the VCB operations can also produce internal resonances between the inductive system components and cable systems [12] which in consequence can highly exceed voltage ratings of insulation systems of components [13].

These interactions between VCBs and other power system components such as transformers and cables are investigated in various power system transient studies [8, 9, 12, 15, 16, 17], for which a simulation model of the VCB is in use based on the concept introduced in [14]. The concept is based on a simulation algorithm employing breakdown voltage characteristics (BDV), the measurement of which is reported in this paper.

S. Stoczko (e-mail: szymon.stoczko@pw.edu.pl), M. Szewczyk (e-mail: marcin.szewczyk@pw.edu.pl), R. Szreder (e-mail: radoslaw.szreder@pw.edu.pl) are with Electrical Power Engineering Institute, Warsaw University of Technology, Koszykowa 75 St., 00-662 Warsaw, Poland. W. Chmielak is with Elektrometal Energetyka S.A., Działkowa 67 St., 02-234 Warsaw, Poland (e-mail: waldemar.chmielak@elektrometal-energetyka.pl). Z. Pochanke is professor emeritus of Warsaw University of Technology (e-mail: zbigniew.pochanke@pw.edu.pl). Corresponding author: M. Szewczyk.

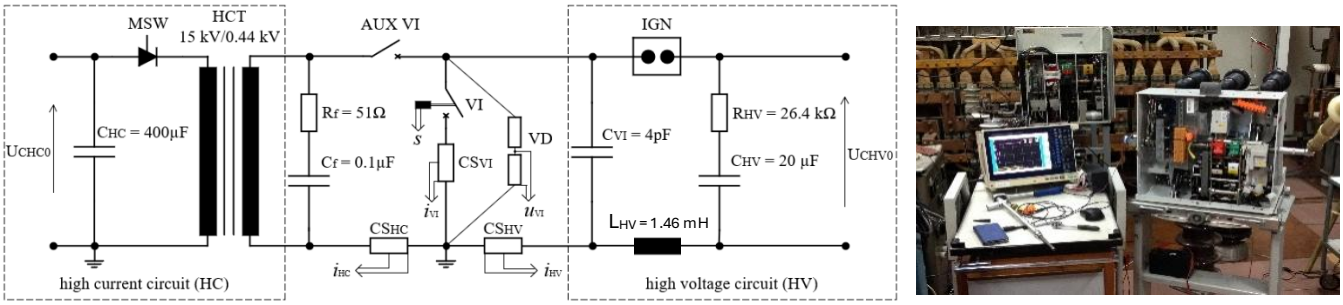

Fig. 1. Test set-up with high current and high voltage circuits (a); vacuum circuit breaker 12kV/1250A/31.5kA under test (b); VI / AUX VI – Vacuum Interrupter under test / auxiliary VI, HCT – high current transformer, MSW – thyristor making switch, IGN – triggered spark gap, C_{HC}/C_{HV} – capacitor banks in high current/voltage circuits pre-charged with voltages U_{CHC0}/U_{CHV0}, L_{HV} – inductance in high voltage circuit, R_f/C_f – RC filter, $CS_{HC}/CS_{HV}/CS_{VI}$ – current shunts for measuring i_{HC}/i_{HV} in high current/voltage circuits and current i_{VI} at VI, VD – voltage divider with ratio 1:200 for measuring voltage u_{VI} across VI, C_{HV}/R_{HV} – capacitor/resistor shaping voltage across VI according to formula (2), s – contact travel curve measured with Wheatstone bridge, C_{VI} – VI voltage shaping capacitor.

II. Paper Aim and Scope

Our aim is to report on a test circuit allowing to obtain the breakdown voltage characteristics after current interruption process thus upon the actual post-current conditions occurring in the VI unit. These conditions depend on the arc current magnitude and phase, arcing time and the actuator characteristics defining the VI's moving contact travel curve. The test circuit is a combination of the high current circuit as per IEC Std. 62271-101 [21] to reproduce the 50-60 Hz current trace before current interruption at current zero, and the high voltage Rabus type circuit [20] to reproduce voltage stress after current zero time instance.

In many works on power system transient studies the BDVs are measured in only Rabus high voltage test set-up [20], providing the so-called "cold" characteristics, i.e., not involving current interruption process proceeding development of voltage breakdown strength of the contact gap and thus not involving effects imposed on the contact system by the breaking current. This is the case in, e.g., the studies on the VCB-induced overvoltages in distribution power grids with photovoltaic generation systems [18], offshore windfarm generation systems [12], development works on transformer overvoltage protection methods [8], and analyses of voltage escalations during current breaking operations of generator VCBs [19]. In some other works, the current conditions are reproduced from onsite or laboratory systems representing specific system configurations [27, 28] or, as in [26], from the measurement results published in classical literature [1].

The test circuit presented in our manuscript proposes a modification of the high-voltage part of the synthetic circuit defined in IEC Std. 62271-101 [21]. In the proposed test circuit, an additional capacitance (C_{VI}, see Fig.1) is introduced into the high-voltage part, charged from a voltage source (U_{CHV0}, see Fig. 1) and connected in parallel to the contacts of the interrupter under test (VI, see Fig. 1). This system, referred to as the Rabus circuit, aims to reproduce the recovery voltage with envelope parameters defined by the IEC Std. 62271-100 [23] while ensuring that, in the event of arc ignition, the arc is extinguished immediately, allowing the recovery voltage to continue building up. In this manner, after the current passes through zero, the recovery voltage between the contacts of the test interrupter (VI) rises, causing repetitive arc ignitions of short duration and consequently low charge.

The low charge in the arc ignitions between the opening contacts of the tested interrupter (VI) after current zero ensures that these repetitive ignitions do not alter the state of the contact surface under no-current conditions, particularly in cases where this is relevant for determining the breakdown voltage (BDV) characteristics following current interruption. Additionally, the current supplied by the high-current part of the circuit prior to zero allows for measuring the breakdown voltage characteristics under post-current conditions (the so-called hot BDV). Thus, the BDV of the interrupter (VI) can be measured under conditions closely resembling the actual circuit breaker operation during current switching process.

In the proposed test circuit, by appropriately modifying the high-current and high-voltage sections, one can replicate switching conditions of the systems described in, e.g., [9, 12, 15, 17, 29, 30, 31], as well as other conditions. For instance, to measure the BDV under switching conditions of a cable line with various lengths and parameters, in the proposed test set-up it is sufficient to adjust the parameters of high-current and high-voltage parts appropriately, eliminating the need for tests involving specific cables components.

To illustrate the method here presented, we report on the measurement results of voltage breakdowns for a commercial 12kV/1250A/31.5kA vacuum circuit breaker (rated voltage / rated continuous current / rated short circuit current) and then present how these results can be applied to a breaker with the same characteristics of the VI and same current conditions, but with different mechanical characteristics of the breaker-specific actuator system than the one used in testing.

III. Modeling of Breakdown Voltage Characteristics for Power System Transient Studies

A black-box model of VCB was proposed in [14] for power system transient studies to investigate interaction of overvoltages originated from voltage breakdowns in VCB with insulation systems of other power system components. The key part of the model is a nonlinear resistive element controlled based on the simulated instantaneous values of the voltage and

the current at the breaker terminals, controlled in accordance with the implemented in the model internal VI breakdown voltage characteristics (BDV). The BDV is a voltage function of the breaker operation time fitted to the breakdown voltages occurring after current interruption at current zero. For the contact gaps that are typical for medium voltage VIs (e.g., 14 mm for 12 kV breaker as used in this paper) and for the initial phase of the contact separation (approx. 1 ms), the BDV can be approximated as a linear function of time t, given by the formula [14, 17]:

$$u_{\mathrm{B}}(t) = a \cdot (t - t_{\mathrm{CP0}}) + b = a \cdot t_{\mathrm{CP}} + b, \qquad (1)$$

where: t is the measurement or the simulation time of a VCB operation, t_{CP0} is the time instance of the VI contact parting, $t_{\mathrm{CP}} = t - t_{\mathrm{CP0}}$ is the opening time starting at the time instance t_{CP0} of the VI contact parting, a in kV/ms is a slope factor of the BDV (rate of rise) and b in kV is the initial voltage breakdown at t_{CP0} (see also Appendix).

The linear formula (1) is a rough approximation of the actual BDV [14], valid only for the initial phase of the moving contact. In principle, the BDV is dependent upon the actual interruption process, the physical features of the VI design linked with different arc quenching capabilities in different phases of the contact separation, and the travel curve of the moving contact which is nonlinear and dependent upon the breaker-specific mechanical actuator system. Moreover, the BDV has statistical variation [14] which can be implemented in the model by statistical variation of the parameters in the BDV formula [26], such as a and b in (1). We use formula (1) in this paper to illustrate the measuring procedure with the test circuit here reported.

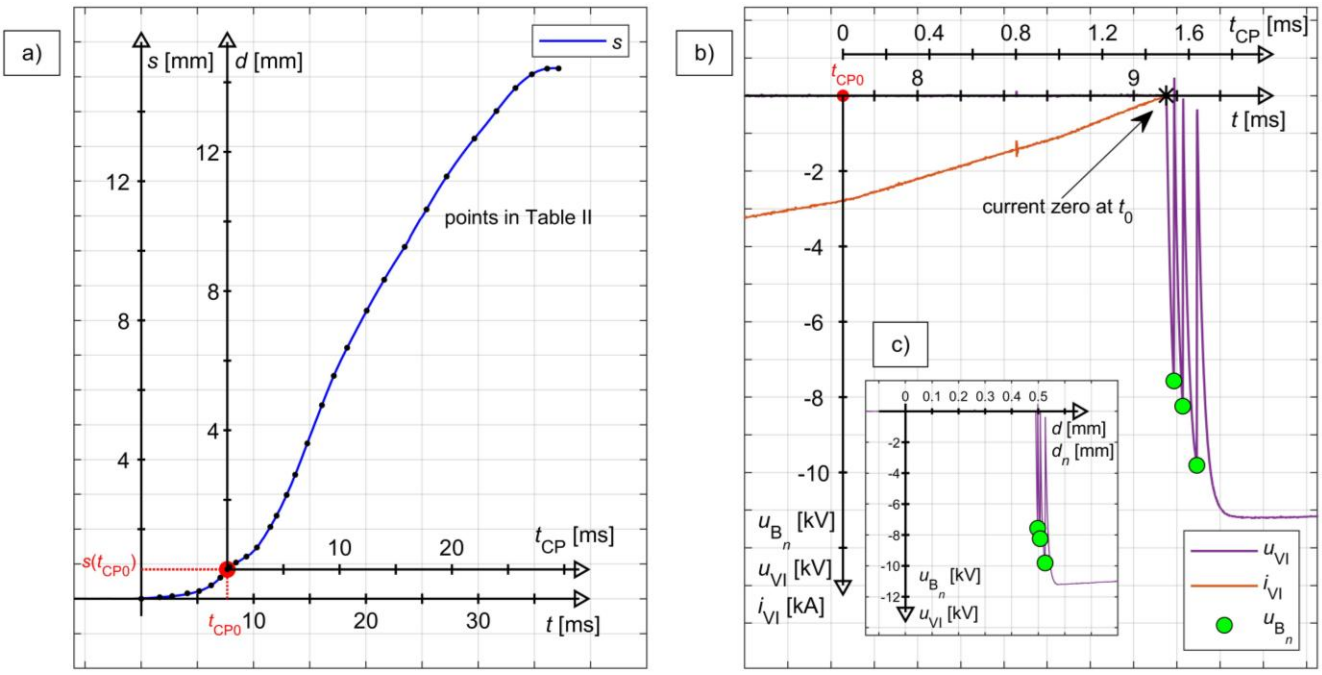

Fig. 2. Test procedure: a) $s(t)$ – moving contact displacement at pushing rod (see Fig. 3) as a function of time t; $d(t_{\mathrm{CP}})$ – contact gap in VI as a function of time t_{CP}; b) $u_{\mathrm{VI}}(t_{\mathrm{CP}})$ – voltage trace at VI contact gap as a function of t_{CP}; $u_{\mathrm{B}_n}(t_{\mathrm{CP}_n}) = u_{\mathrm{VI}}(t_{\mathrm{CP}_n})$ – n-th voltage breakdowns at time instance t_{CP_n} equal to voltage trace at VI contact gap at time instance t_{CP_n}. The breakdown voltage characteristics $u_{\mathrm{B}}(t_{\mathrm{CP}})$ is a fit to $u_{\mathrm{B}_n}(t_{\mathrm{CP}_n})$, here approximated with formula (1).

IV. Experimental Test Circuit for Measurement of VCB Breakdown Voltage Characteristics

A. Synthetic test circuit with Rabus voltage part

The measurements are conducted in a test circuit shown in Fig. 1, in which a high current part was arranged in accordance with synthetic test circuit method as defined in IEC Std. 62271-101 [21] and then combined with the Rabus voltage circuit according to [20]. The Rabus part provided voltage escalation and then repetitive ignitions of switching arc after current interruption at current zero.

The high current and the high voltage are generated (see Fig. 1) by discharging of high voltage capacitor banks, C_{HC} and C_{HV}, respectively. The capacitor banks are pre-charged before testing by individual voltage chargers. Voltage levels at the capacitor banks correspond to the rated voltage of the VI under test (in our case limited to 11 kVpeak). The high current circuit is triggered with a dedicated making switch MSW installed at the primary side of the high current transformer HCT allowing lower current requirements imposed on the making switch MSW. The 50-60 Hz equivalent frequency of a half sine wave is adjusted by the high current transformer HCT inductance and the capacitance of the C_{HC} capacitor bank. The current peak value at the VI under test is controlled by the pre-charge voltage of the C_{HC} capacitor and the ratio of high current transformer HCT. The high voltage is generated by discharging of C_{HV} capacitor via L_{HV} inductor by the triggered spark gap IGN.

Based on the synthetic testing procedure [21], the two poles of the breaker are connected in series, one of which serving as a VI under test, and the other one was an auxiliary AUX VI. The breaker actuator is triggered milliseconds before the high

current half sine wave is initiated. The tested VI and the AUX VI contacts part before current zero, and the switching arc is established in the contact gaps of both VIs. At current zero the arc is extinguished in both VIs, hence the AUX VI separates the high current circuit form the tested VI and from the rest of the circuit. This allows safe operation of the high current transformer HCT requiring voltage protection due to its high current but low voltage insulation ratings. As an additional protection of the HCT, an RC filter parallel to the secondary side of the transformer is used. Following the separation time instance, the spark gap IGN is ignited, and the high voltage is applied across the VI contact gap.

Unlike to the standardized synthetic test circuits as defined in IEC Std. 62271-101 [21, 22], in our circuit the high voltage stress across the VI contact gap is applied exponentially, following the transient process in an RC-type circuit (namely $R_{\mathrm{HV}}C_{\mathrm{VI}}$, see Fig. 1). The voltage rise is shaped by the capacitor C_{VI} connected in parallel to the VI and the resistor R_{HV}, according to formula:

$$u_{\mathrm{VI}}(t_{\mathrm{CP}}) = U_{\mathrm{CHV0}}\left(1 - e^{-\frac{t-t_0}{R_{\mathrm{HV}}C_{\mathrm{VI}}}}\right), \qquad (2)$$

where: u_{VI} is the voltage imposed across the VI under test contact system (generated in the high voltage circuit), t_0 is the time instance of zero current crossing, C_{VI} and R_{HV} are, respectively, capacitor and resistor components shaping voltage across the VI under test, U_{CHV0} is the pre-charge voltage of C_{HV} capacitor.

In our measurements the initial rate of rise of the voltage given by formula (2) was set to $0.3\ \mathrm{kV/us}$, which was referred to the highest rate of rise of recovery voltage (RRRV) of $0.345\ \mathrm{kV/us}$ as defined in IEC Std. 62271-100 [23] for 12 kV breaker at the T100 test duty conditions.

The peak value of the voltage stress imposed across the VI contact gap is controlled by the pre-charge voltage of the high voltage C_{HV} capacitor bank in high voltage circuit (Fig. 1). When the voltage stress exceeds the contact gap withstand voltage, a voltage breakdown occurs initiated by the switching arc ignition in the VI contact system, such as the one given by the approximate formula (1).

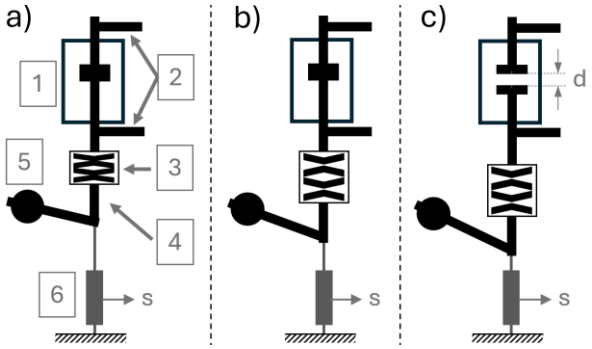

Fig. 3. VI moving contact during opening operation: a) VI closed position; b) VI contact spring release stage; c) contact parting stage; 1 – VI, 2 – current terminals, 3 – contact spring, 4 – pushing rod, 5 – drive shaft, 6 – potentiometric position transducer.

Ultimately, the breakdown voltage characteristics $u_{\mathrm{B}}(t_{\mathrm{CP}})$ of the VCB is a voltage function fitted to the subsequent voltage breakdowns (arc reignitions) and expressed as a function of contact parting time t_{CP}.

B. Test procedure

Until the VI contacts start to separate, the movement of the VCB driving rod is not synchronized with the movement of the VI moving contact (see Fig. 2 and 3). To express the breakdown voltage characteristics as a function of contact parting time, $u_{\mathrm{B}}(t_{\mathrm{CP}})$, it is necessary to consider the contact parting time instance t_{CP0}, which delays the separation of the VI contacts compared to the actuator rod movement, due to the relaxation of the stack of compression springs.

Therefore, we first measured (see Fig. 2 and 3) the moving contact displacement at pushing rod as a function of time t, s(t). Then we used contact parting time, t_{CP0}, to obtain VI contact gap as a function of contact parting time t_{CP}, $d(t - t_{\mathrm{CP0}}) = d(t_{\mathrm{CP}})$. The voltage trace at the VI contact gap as a function of contact parting time, $u_{\mathrm{VI}}(t_{\mathrm{CP}})$ was then used to detect n time instances t_{CP_n} of the voltage breakdowns, for which the breakdown voltages were recorded, $u_{\mathrm{B}_n}(t_{\mathrm{CP}_n}) = u_{\mathrm{VI}}(t_{\mathrm{CP}_n})$. The breakdown voltage characteristics $u_{\mathrm{B}}(t_{\mathrm{CP}})$ is then a fit to $u_{\mathrm{B}_n}(t_{\mathrm{CP}_n})$, for which in our case we used approximation given in formula (1). For higher u_{VI} and observed higher breakdown voltages polynomial fit can be used instead [26], [27].

The VCB contact travel curve $s(t_{\mathrm{CP}})$ and the voltage breakdowns $u_{\mathrm{B}_n}(t_{\mathrm{CP}_n})$ were measured using Wheatstone potentiometer bridge, in which an adjustable linear resistor was mechanically fixed to the VI pushing rod (see Fig. 3). The displacement of the VI moving contact was recorded as the voltage imbalance of the bridge. Knowing the imbalance voltage and the pushing rod displacement, the V/mm scaling factor was found allowing to scale the bridge imbalance voltage to millimeters of the VI contact distance.

C. Synchronizing of high current and high voltage circuits

The measurement started from sending a triggering signal to an actuator coil of the tested VCB. Knowing the self-time of the VCB actuator system, another impulse was then sent to the making switch MSW, initiating a half-sine trace of 50Hz high current through two poles of the breaker connected in series, followed by the contact separation and ignition of the switching arc in both the VI under test and the AUX VI. After current zero crossing, the high voltage circuit was separated from the high current circuit by the AUX VI. The spark gap IGN was triggered right after zero current crossing to impose the high voltage from the high voltage circuit on the VI under test.

For synchronizing of the voltage circuit, the triggered spark gap IGN was used of a conventional design. For synchronizing the high current circuit, a dedicated thyristor-based making switch MSW was designed based on $N = 2x5$ screw-type 1400V/100A T51-100-14-50-JXA thyristors arranged in 2 anti-parallel connected stacks (each stack formed by 5 serially connected items, therefore allowing each stack to withstand voltage up to 7 kV). The anti-parallel connection of the individual thyristor stacks allowed bidirectional current

conduction. The thyristors in each stack were simultaneously ignited to avoid exceeding the voltage ratings of individual thyristors and consequently a failure of all thyristors in a row. The triggering was initiated by a fiber optic impulse applied to the FET transistor on the high voltage side of the multi-winding transformer MWT, which then energized the flyback DC/DC converter. The current at the primary side of the multi-winding transformer MWT induced simultaneously the current in all magnetically coupled secondary windings supplying thyristors via RC voltage dividers. The RC voltage dividers were connected to each thyristor in stack for uniform voltage distribution in both steady and transient states.

V. Measurement of BDV for 12kV VCB

A. Test conditions

For presenting a test circuit and the test procedure here reported, we measured the BDV of a 12 kV VI. The VI under test was one pole of a commercial 12kV/1250A/31.5kA VCB with a spring operated actuator system, as shown in Fig. 1 and 3. The actual measurements followed pre-conditioning the VI contacts with a peak current of 5 kA (approximately 10% of the nominal breaking current of the VI under test), until no impact of the breaking current on voltage breakdowns was observed. This allowed to smooth and clean adsorbed gases, oxides and microparticles from the contact surfaces, thereby stabilizing breakdown voltage conditions in the following measurements [24]. Then the measurements were conducted for the breakdown voltages after breaking current of 9 kApeak standing for approximately 20% of nominal breaking current of the VCB under test. The voltage during tests was limited to 11 kVpeak due to lab limitations. This value stands for a half of the voltage defined in IEC Std. 62271-100 [23] for T100 test.

For recording of current i_{HC} in high current circuit and current i_{VI} in the VI (see Fig. 1) two 800 μΩ current shunts were used. A 1 Ω shunt resistor was used for recording of current i_{HV} in high voltage circuit. An RC voltage divider with 1:200 ratio was used for recording of voltage u_{VI} at the VI under test.

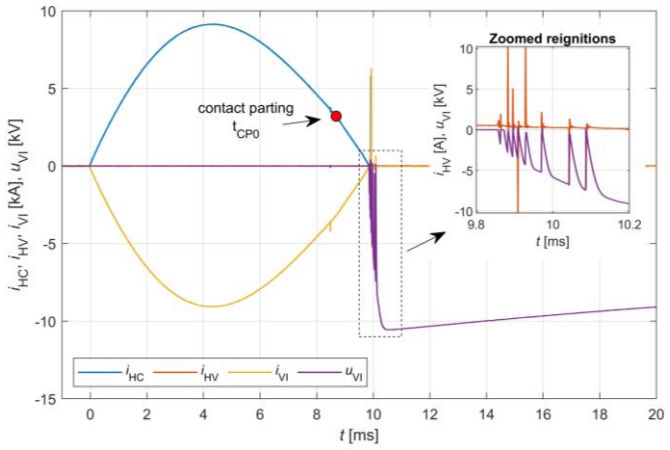

Fig. 4. Current and voltage traces recorded during testing with zoomed-in reignitions (see also Fig. 5) and red circle indicating time instance of VI contact parting (see also Fig. 6); i_{HC} /i_{HV} are currents in high current/voltage circuits, i_{VI} is current at VI, u_{VI} is voltage across VI, t is time of recording.

B. Overall current and voltage traces

Fig. 4 shows example of current and voltage traces recorded. The half-sine waveform of 50 Hz current with 9 kA peak value starts at 0 ms. The contact parting of the VI is marked with red circle. After current zero crossing, the voltage u_{VI} is applied across the VI contacts as given by the formula (2). When the voltage u_{VI} across the VI exceeds the VI's contact gap breakdown voltage, the switching arc is ignited in a form of repetitive reignition process. The time between tripping signal and the time instance of the contact parting t_{CP0} are separated, thus the reignitions are expressed as a function of contact parting time $t_{\mathrm{CP}} = t - t_{\mathrm{CP0}}$.

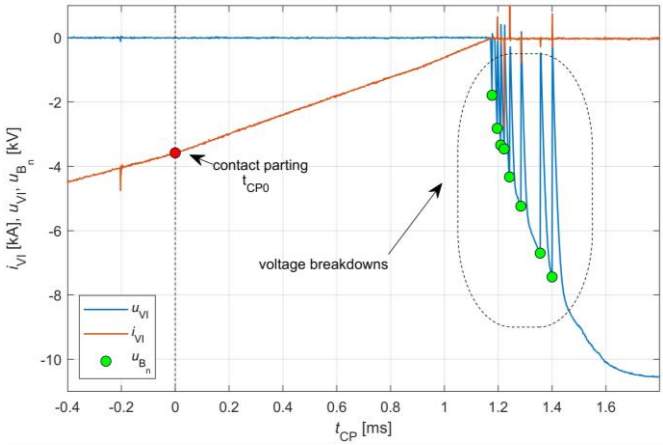

Fig. 5. Measured voltage across VI under test, $u_{\mathrm{VI}}(t_{\mathrm{CP}})$, for the test run shown in Fig. 4; red circle indicates time instance of VI contact parting (see also Fig. 6), green circles indicate switching arc reignitions at $u_{\mathrm{Bn}}(t_{\mathrm{CPn}})$; $i_{\mathrm{VI}}(t_{\mathrm{CP}})$ is current at VI, $u_{\mathrm{VI}}(t_{\mathrm{CP}})$ is voltage across VI, t_{CP} is contact parting time.

Fig. 5 shows the reignitions obtained from the voltage traces shown in Fig. 4, plotted as a function of contact parting time t_{CP}. The reignitions are initiated by the voltage $u_{\mathrm{VI}}(t_{\mathrm{CP}})$ across the VI under test, constituting set of voltage breakdowns $u_{\mathrm{Bn}}(t_{\mathrm{CPn}})$.

C. Detection of contact parting

High withstand voltage capability of VIs and therefore short contact gaps are unquestionable advantages of vacuum as switching arc quenching technology of VCBs. These qualities, however, impose high requirements on accuracy of contact movement measurement during testing of the voltage reignitions occurring at the initial stage of contact separation. The time instance of contact parting t_{CP0} cannot be directly measured by measuring contact travel curve on the synchronization shaft or even by displacement measurement on insulated end of VCB poles pushing rods (see Fig. 3), which is due to the spring system located between the rod shaft and the VI moving contact.

Fig. 6 shows contact parting detection applied for current trace shown with red dot in Fig. 4 and 5. The contact parting initiates the switching arc in the VI contact gap. The associated voltage drop appearing across the contact gap due to arc ignition influences the current trace i_{VI} during the high current phase, which can be then detected from variation in the current trace by differentiation and filtering procedure. The current trace i_{VI} is subjected to averaging filter, then differentiated, and then

filtered again. The drop in the filtered current derivative indicates the time instance of the VI contact separation. The identified contact parting time instance t_{CP0} is marked with a red circle in Figs. 4-6.

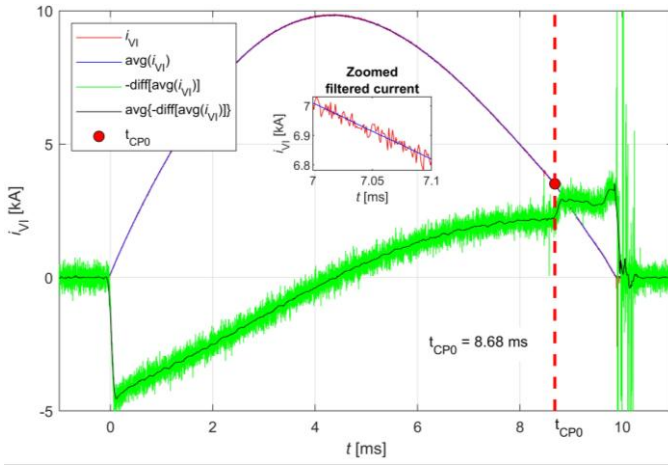

Fig. 6. Contact parting detection applied for current trace shown in Fig. 4; t_{CP0} indicated with red circle is the time instance of contact parting.

VI. Measured Breakdown Voltage Characteristics

A. Voltage breakdowns in VI

Fig. 7 shows voltage breakdowns u_{B_n} measured in 10 runs, plotted as a function of contact parting time t_{CP_n} with a linear BDV characteristics fitted, $u_{\mathrm{B}} = u_{\mathrm{B}}(t_{\mathrm{CP}})$, according to formula (1). Although the formula (1) used is an approximation of the actual BDV, its slope factor 21.14 kV/ms well agrees with the value 20 kV/ms reported in [18] and [25]. Considering many conditions determining the actual BDV of the VI with given design and ratings (switching history, arching time, switching current rms value), measurements for many switching operations in given conditions are necessary to define the actual BVD formula.

The raw data of the voltage breakdowns $u_{\mathrm{B}_n}(t_{\mathrm{CP}_n})$ shown in Fig. 7 is given in Table I.

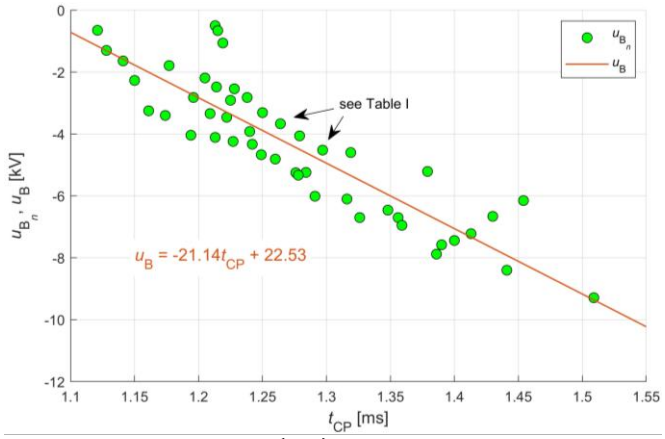

Fig. 7. Breakdown voltages $u_{\mathrm{B}_n}(t_{\mathrm{CP}_n})$ as a function of contact parting time t_{CP} (for 10 runs) with linear BDV characteristics $u_{\mathrm{B}}(t_{\mathrm{CP}})$ fitted according to formula (1). Raw data of voltage breakdowns $u_{\mathrm{B}_n}(t_{\mathrm{CP}n})$ are given in Table I.

B. Contact travel curve

The BDV characteristics shown in Fig. 7 expressed as a function of contact parting time, $u_{\mathrm{B}}(t_{\mathrm{CP}})$, can be directly implemented in the time-domain simulation software for power system studies, such as EMTP or PSCAD (see e.g. [12]). Such representation is, however, dependent upon the VCB contact travel curve, $s = s(t)$, which is a nonlinear function of the breaker operation time t and is specific to mechanical characteristics of the breaker actuator system. Therefore, the BDV provided in a form of $u_{\mathrm{B}}(t_{\mathrm{CP}})$ is relevant to a VI operated in an actuator system of specific design only (as well as the current conditions and VI switching history), for which the actual characteristics was measured.

To obtain a BDV characteristics of the VI that is independent from mechanical characteristics of the breaker actuator system, which can be then re-used for any VCB actuator system, the time dependent characteristic $u_{\mathrm{B}}(t_{\mathrm{CP}})$ can be converted to a function of the VI contact gap d: $u_{\mathrm{B}} = u_{\mathrm{B}}(d)$, see Fig. 2. The contact gap d is established based on the measured contact travel curve s using formula:

$$d(\mathrm{t_{CP}}) = s(t_{\mathrm{CP}}) - s(t_{\mathrm{CP0}}), \tag{3}$$

where: $s(t_{\mathrm{CP}})$ is a contact travel curve as a function of contact parting time, and $s(t_{\mathrm{CP0}})$ is the contact travel curve at the time instance of the contact parting. This allows to neglect contact move before contact parting due to, e.g., release of the contact compression spring system (see Fig. 3).

The BDV characteristics represented as a function of contact gap, $u_{\mathrm{B}} = u_{\mathrm{B}}(d)$, can be further converted to a form relevant to any VCB actuator system characterized with a design-specific contact gap curve $d = d(t_{\mathrm{CP}})$.

Fig. 8 shows an example of a single run measurement of voltage $u_{\mathrm{VI}}(t_{\mathrm{CP}})$ across the VI as a function of contact parting time t_{CP} (see Fig. 8a), the contact travel curve $s(t_{\mathrm{CP}})$ measured as a function of contact parting time t_{CP} (see Fig. 8b), and the voltage $u_{\mathrm{VI}}(d)$ across the VI expressed as a function of contact gap d (see Fig. 8c) obtained based on $u_{\mathrm{VI}}(t_{\mathrm{CP}})$ and $s(t_{\mathrm{CP}})$.

The distortion of the travel curve s in proximity of the voltage breakdowns was corrected with the use of the reference contact distance s_{ref} (see Fig. 8b). The s_{ref} was measured at the non-reignition conditions without voltage supplied after zero current crossing and then the s_{ref} curve was fitted to the measured signal s allowing to overcome the disrupted region. In Fig. 8a and Fig. 8d voltage breakdowns u_{Bn} are indicated as functions of, respectively, contact parting time t_{CP} and contact gap d_n. The contact travel curve s was used to transfer time instances $t_{\mathrm{CP}n}$ of voltage breakdown reignitions $u_{\mathrm{B}n}$ into the corresponding contact gap d.

Fig. 9 shows voltage breakdowns $u_{\mathrm{B}n}(d_n)$ for 10 runs, plotted as a function of contact gap d based on the $u_{\mathrm{B}n}(t_{\mathrm{CP}n})$ shown in Fig. 7 and travel curve $s = s(t_{\mathrm{CP}})$ shown in Fig. 8b. A linear BDV characteristics (1) is fitted, $u_{\mathrm{B}}(d)$, with the slope factor $69.9\ \mathrm{kV/mm}$ which agrees with the value $20\ \mathrm{kV/ms}$ reported in [18] and [25].

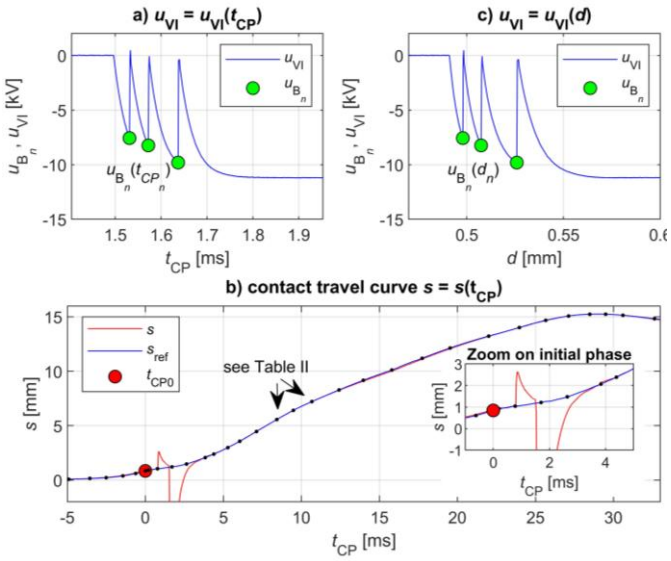

Fig. 8. Voltage u_{VI} across the VI recorded as a function of contact parting time t_{CP} (a); contact travel curve s recorded as a function of contact parting time t_{CP} (b); voltage u_{VI} expressed as a function of contact gap d (c); u_{B_n} – voltage breakdowns as a function of contact parting time, $u_{Bn}(t_{CPn})$ and as a function of contact gap $u_B(d_n)$, t_{CP0} – time instance of contact parting, s_{ref} – reference contact distance measured at non-reignition conditions.

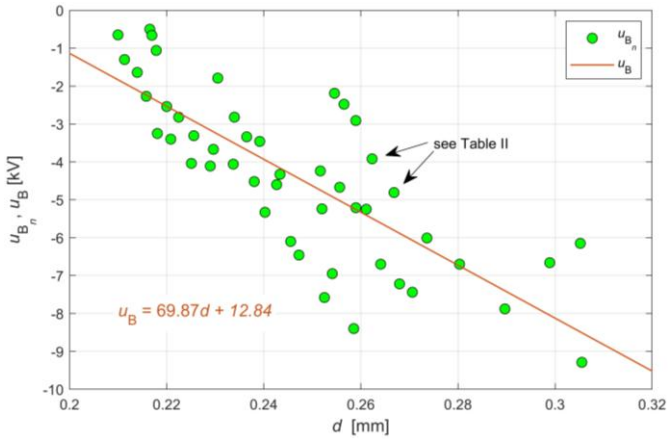

Fig. 9. Breakdown voltages $u_{B_n}(d_n)$ as a function of contact gap d, obtained for contact travel curve shown in Fig. 8 from breakdown voltages u_B shown in Fig. 7 (10 runs) as a function of contact parting time t_{CP}, with linear BDV characteristics $u_B = u_B(d)$ fitted. Raw data of voltage breakdowns $u_{B_n}(d_n)$ are given in Table II.

Table I shows raw data of the recorded voltage breakdowns $u_{Bn}(t_{CPn})$ and $u_{Bn}(d_n)$, as shown in, respectively, Fig. 7 and Fig. 9. Table II shows raw data of contact travel curve s and contact gap d as a function of contact parting time t_{CP}, as shown in, respectively, Fig. 8b and Fig. 8c.

TABLE I
RAW DATA OF RECORDED VOLTAGE BREAKDOWNS $u_{B_n}(t_{CP_n})$ AND $u_{B_n}(d_n)$, AS SHOWN IN FIG. 7 AND FIG. 9

d_n[mm]	t_{CP_n}[ms]	u_{B_n}[kV]	d_n[mm]	t_{CP_n}[ms]	u_{B_n}[kV]
0.252	1.227	-4.240	0.259	1.441	-8.400
0.256	1.249	-4.670	0.255	1.205	-2.190
0.261	1.276	-5.250	0.257	1.214	-2.480
0.306	1.509	-9.290	0.259	1.225	-2.910
0.231	1.177	-1.790	0.262	1.240	-3.920
0.234	1.196	-2.820	0.267	1.260	-4.810
0.236	1.209	-3.340	0.274	1.291	-6.010
0.239	1.222	-3.460	0.280	1.326	-6.700
0.243	1.242	-4.330	0.290	1.386	-7.880
0.252	1.284	-5.240	0.299	1.430	-6.660
0.264	1.356	-6.700	0.305	1.454	-6.150
0.271	1.400	-7.440	0.210	1.121	-6.50
0.217	1.213	-5.000	0.211	1.128	-1.300
0.217	1.215	-6.600	0.214	1.141	-1.640
0.218	1.219	-1.060	0.216	1.150	-2.270
0.220	1.228	-2.540	0.218	1.161	-3.250
0.222	1.238	-2.820	0.221	1.174	-3.400
0.226	1.250	-3.310	0.225	1.194	-4.040
0.230	1.264	-3.670	0.229	1.213	-4.110
0.234	1.279	-4.060	0.240	1.278	-5.330
0.238	1.297	-4.520	0.246	1.316	-6.100
0.243	1.319	-4.600	0.254	1.359	-6.950
0.247	1.348	-6.460	0.259	1.379	-5.210
0.252	1.390	-7.580	0.268	1.413	-7.220

VII. CONCLUSIONS

Breakdown voltage characteristics (BDV) of a vacuum circuit breaker (VCB) depends on the design of the Vacuum Interrupter (VI), the mechanical characteristics of the VCB actuator system, and the contact system condition immediately after current breaking interruption at current zero. Therefore, the BDV should be obtained from a test system involving a VCB operating at a given voltage and current conditions, either in full scale laboratory or on-site measurements. These characteristics are typically not available for modeling and simulation studies of power system transients and can be provided with the test circuit reported in this paper.

TABLE II
RAW DATA OF CONTACT TRAVEL CURVE s AND CONTACT GAP d AS A FUNCTION OF CONTACT PARTING TIME t_{CP}, AS SHOWN IN FIG. 8B AND FIG. 8C

t_{CP_n}[ms]	s_n[mm]	d_n[mm]	t_{CP_n}[ms]	s_n[mm]	d_n[mm]
-6.018	0.000	0.000	8.426	5.562	4.717
-4.905	0.075	0.000	9.485	6.405	5.560
-3.554	0.155	0.000	10.670	7.213	6.368
-2.507	0.220	0.000	12.411	8.279	7.434
-1.438	0.385	0.000	13.970	9.168	8.323
-0.617	0.607	0.000	15.794	10.113	9.267
0.000	0.845	0.000	17.740	11.188	10.343
0.201	0.916	0.071	19.528	12.135	11.290
0.780	1.041	0.196	22.000	13.225	12.379
1.704	1.212	0.366	23.965	14.016	13.170
2.638	1.475	0.629	25.656	14.677	13.831
3.836	2.065	1.219	27.120	14.823	13.978
4.388	2.386	1.541	28.479	15.071	14.226
5.286	2.982	2.137	29.498	15.142	14.296
6.048	3.564	2.719	30.604	15.234	14.389
7.122	4.463	3.618	32.623	15.240	14.394

This paper reports on a modified synthetic test circuit combined with a Rabus high voltage circuit, synchronized to measure voltage breakdowns after the current interruption process. The individual points of the breakdown voltage characteristics are determined without altering the state of the tested object due to the low-energy arc ignitions. In contrast, in dedicated labs or in systems representing specific switching conditions, each arc ignition modifies the tested object primarily by altering the contact surface of the vacuum interrupter, which is due to the fact that the ignitions are fully energized, supplied from the external circuit. The proposed approach enhances the possibility of conducting in-depth measurements of the VI breakdown voltage characteristics in a standardized synthetic test setup. Any lab with a synthetic test circuit can modify it, and the paper demonstrates the consequences of this modification and reports on value it provides. By introducing a modification to the standardized synthetic test circuit, breakdown voltage characteristics can be measured without changing the essence of the synthetic testing, with parameters aligned to the requirements of IEC Std. 62271-101.

The method presented involves first measuring the BDV characteristics of the VI with a given actuator system. The characteristics is obtained by the breakdown voltages as a function of the dis-placement of the VI moving contact. The displacement is determined by the movement of the pushing rod, which is connected to a drive mechanism consisting of a spring and a tensioning system. Subsequently, to determine the inherent BDV characteristics of the VI without the drive mechanism, the previously measured BDV characteristics as a function of the pushing rod displacement is converted into a BDV as a function of the VI contact gap. Once the BDV characteristics as a function of the contact gap is obtained, it can be transformed back into the BDV characteristics of the VI but with another drive mechanism by applying the traveling curve characteristic of the new drive, which can be measured separately using a no-voltage measurement. In this way, the BDV characteristics of the VI with a new drive mechanism can be obtained.

The measurement procedure is presented for a commercial 12kV/1250A/31.5kA vacuum circuit breaker. The measured time-domain breakdown voltage characteristics are converted into VI-specific function of the VI contact gap, which, together with the breaker contact travel curve (which depends on the mechanical characteristics of the breaker's actuator system), allows for the implementation of these characteristics for a breaker actuator system of any design. Such characteristics can then serve as an input for the EMTP or PSCAD simulations to investigate transient interactions between VCB and other power system components.

Detecting the moment of contact separation in a given test run allowed for determining the actual contact gap of the circuit breaker (by defining a dead displacement of the moving contact), which otherwise would be affected by statistical distribution in circuit breaker actuators.

The BDV characteristic here reported are in an initial region of contacts parting, in which linear approximation holds. The slope factor of the linear approximation agrees with the values reported in the literature.

APPENDIX: NOMENCLATURE

t time recorded in measurements
t_0 time instance of current zero crossing
t_{CP0} time instance of contact parting
t_{CP} time starting at the time instance t_{CP0}, $t_{\mathrm{CP}} = t - t_{\mathrm{CP0}}$
t_{CP_n} time instances of voltage breakdowns
s contact travel curve recorded in measurements
d contact gap calculated with use of t_{CP0}
u_{VI} voltage imposed across the VI under test
u_{B_n} voltage breakdown for n-th arc reignition at t_{CP_n}
u_{B} fitted approximation curve to n breakdown voltages u_{B_n}, breakdown voltage characteristics

REFERENCES

[1] P.G. Slade, The Vacuum Interrupter: Theory, Design, and Application, 2nd ed. CRC Press, 2021
[2] R. Renz, D. Gentsch, H. Fink, P. Slade, "Vacuum Interrupters – Sealed For Life," *in 19th International Conference on Electricity Distribution*, 21-24.05.2007, Vienna, CIRED, Paper 0156
[3] Z. Zhang et al., "Anode Spot Threshold Current of Four Pure Metals Subjected to Uniform Axial Magnetic Field in High Current Vacuum Arcs," *IEEE Trans. Plasma Sci*., vol. 45, no. 8, pp. 2135–2143, 2017, doi: 10.1109/TPS.2017.2705171.
[4] A. Logachev, I. N. Poluyanova, K. K. Zabello, Y. A. Barinov, S. M. Shkol'nik, "Cathode Surface State and Cathode Temperature Distribution after Current Zero of Different AMFContacts," *IEEE Trans. Plasma Sci.*, vol. 47, no. 8, pp. 3516–3524, 2019, doi: 10.1109/TPS.2019.2923326.
[5] J. Tang, S. Lu, J. Xie, Z. Cheng, "Contact Force Monitoring and Its Application in Vacuum Circuit Breakers," *IEEE Trans. Power Deliv.*, vol. 32, no. 5, pp. 2154–2161, 2017, doi: 10.1109/TPWRD.2015.2423686.
[6] H. Ejiri et al., "Late Breakdowns Caused by Microparticles after Vacuum Arc Interruption," *IEEE Trans. Plasma Sci.*, vol. 47, no. 8, pp. 3392–3399, 2019, doi: 10.1109/TPS.2019.2917379.

[7] S. Stoczko, M. Szewczyk, Z. Pochanke, W. Chmielak, "Experimental study on field emission current in vacuum interrupter at functional limit of vacuum pressure," *Electr. Power Syst. Res.*, Volume 191, 2021, 106860, doi: 10.1016/j.epsr.2020.106860.

[8] D. Smugala, W. Piasecki, M. Ostrogórska, M. Fulczyk, M. Florkowski, P. Kłys, "Protecting distribution transformers against Very Fast Transients due to switching operation," in 2010 Modern Electric Power Systems conference, 20-22 Sept. 2010, Wroclaw, Poland

[9] D. Smugala, W. Piasecki, M. Ostrogórska, M. Florkowski, M. Fulczyk, O. Granhaug, "Wind Turbine Transformers Protection Method Against High-Frequency Transients," *IEEE Trans. Power Deliv*., Vol. 30, No. 2, April 2015

[10] D. D. Shipp, T. J. Dionise, V. Lorch, W. G. MacFarlane, "Vacuum Circuit Breaker Transients During Switching of an LMF Transformer," *IEEE Trans. Ind. Appl*., Vol. 48, No. 1, January/February 2012

[11] D. D. Shipp, T. J. Dionise, V. Lorch, B. G. MacFarlane, "Transformer failure due to circuit breaker induced switching transients," *IEEE Trans. Ind. Appl*., Vol. 47, No. 2, March/April 2011

[12] T. Kuczek, M. Florkowski, W. Piasecki, "Transformer Switching with Vacuum Circuit Breaker: Case Study of PV Inverter LC Filters Impact on Transient Overvoltages," *IEEE Trans. Power Deliv*., vol. 31, no. 1, 2016, doi: 10.1109/TPWRD.2015.2437199.

[13] *Insulation Co-ordination—Part 1: Definitions, Principles and Rules*, IEC Std. 60071-1:2019, ed. 9.0; IEC: Geneva, Switzerland, 2019.

[14] J. Helmer, M. LIndmayer, "Mathematical modeling of the High Frequency Behavior of Vacuum Interrupters and Comparison with Measured Transients in Power System," in 17th International Symposium on Discharges and Electrical Insulation in Vacuum, Berkeley, 21-26.07.1996, doi: 10.1109/DEIV.1996.545375

[15] T. Abdulahovic, T. Thiringer, M. Reza, H. Breder, "Vacuum Circuit-Breaker Parameter Calculation and Modelling for Power System Transient Studies," *IEEE Trans. Power Deliv*., vol. 32, no. 3, 2007.

[16] J. Kosmac, P. Zunko, "A Statistical Vacuum Circuit Breaker Model for Simulation of Transient Overvoltages," *IEEE Trans. Power Deliv*., vol. 10, no. 1, 1995

[17] Q. Zhou, Y. Cheng, X. Bian, F. Liu, Y. Zhao, Analysis of Restrike Overvoltage of Circuit Breakers in Offshore Wind Farms, *IEEE Trans. Appl. Supercond.*, vol. 26, no. 7, 2016

[18] T. Kuczek, M. Florkowski, "Vacuum Circuit Breaker Switching in Photovoltaic Power Plants – Overvoltage Analyses for Various Topologies and Network Conditions", *Zeszyty Naukowe Wydziału Elektrotechniki i Automatyki Politechniki Gdańskiej*, no. 36

[19] M. T. Glinkowski, M. R. Gutierrez, D. Braun, "Voltage Escalation and Reignition Behavior of Vacuum Generator Circuit Breakers During Load Shedding," *IEEE Trans. Power Deliv*., vol. 12, no. 1, 1997

[20] A. T. Roguski, "Experimental Investigation of the Dielectric Recovery Strength Between the Separating Contacts of Vacuum Circuit Breakers," *IEEE Trans. Power Deliv*., vol. 4, no. 2, 1989, pp. 1063–1069

[21] *High-voltage switchgear and controlgear – Part 101: Synthetic testing*, IEC Std. 62271-101, ed. 3.0, Jul. 2021.

[22] M. Szewczyk, S. Stoczko, A. Zagrajek, W. Chmielak, "Comparative Study of Synthetic Test Circuits for Testing of MV and HV AC Circuit Breakers According to IEC Std. 62271" in Procceedings of Progress in Applied Electrical Engineering Conference (PAEE 2019), Kościelisko, 17-22.06.2019, DOI: 10.1109/PAEE.2019.8789001

[23] *High-voltage switchgear and controlgear – Part 100: Alternating-current circuit-breakers*, IEC Std. 62271-100, Jul. 2021.

[24] P. Spolaore, G. Bisoffi, F. Cervellera, R. Pengo, F. Scarpa, G. Binelle, A. Zanon, "The large gap case for HV insulation in vacuum," *IEEE Trans. Dielectr. Electr. Insul*., vol. 4, no. 4, 1997, doi: 10.1109/94.625353.

[25] Kondala Rao, G. Gajjar, "Development and Application of Vacuum Circuit Breaker in Electromagnetic Transient Simulation," in 2006 IEEE Power India Conference, 10-12 April 2006, New Dehli, India, doi: 10.1109/POWERI.2006.1632503.

[26] A. A. Razi-Kazemi, M. R. Fallah, M. Rostami, F. Malekipour, "A new realistic transient model for restrike/prestrike phenomena in vacuum circuit breaker," *Int. J. Electr. Power Energy Sys.*, vol. 117, 2020, 105636, doi: 10.1016/j.ijepes.2019.105636

[27] Q. Yang, S. Chen, X. Zeng, G. Wei, H. Liu and T. Chen, "Suppression Measures for Overvoltage Caused by Vacuum Circuit Breaker Switching Off 10-kV Shunt Reactor," *IEEE Trans. Power Deliv.*, vol. 35, no. 2, pp. 540-548, April 2020, doi: 10.1109/TPWRD.2019.2912663

[28] Y. Guo, X. Jiang, Y. Chen, M. Zheng, G. Liu, X. Li, W. Tang, "Reignition overvoltages induced by vacuum circuit breakers and its suppression in offshore wind farms," *Int. J. Electr. Power Energy Sys.*, vol. 122, 2020, 106227, doi: 10.1016/j.ijepes.2020.106227

[29] Q. Sun et al., "Investigation on Multiple Reignitions Caused by Vacuum Circuit Breaker Switching Off Shunt Reactor Considering Contact Travel in Offshore Wind Farms," in IEEE Transactions on Power Delivery, vol. 38, no. 4, pp. 2360-2371, Aug. 2023, doi: 10.1109/TPWRD.2023.3241407

[30] Z. Zheng et al., "Investigation on Power Frequency Following Current for Vacuum Circuit Breaker Interrupting Shunt Reactor in Offshore Wind Farms," in IEEE Transactions on Power Delivery, vol. 39, no. 1, pp. 306-316, Feb. 2024, doi: 10.1109/TPWRD.2023.3334287

[31] Z. Zheng et al., "Investigation on overvoltage caused by vacuum circuit breaker switching off shunt reactor in offshore wind farms." in High Voltage, vol. 7, no. 5, pp. 936-949l, May 2022, doi: 10.1049/hve2.12231